Redox Biology 44 (2021) 102016

Contents lists available at ScienceDirect

Redox Biology

journal homepage: www.elsevier.com/locate/redox

Histidine dipeptides are key regulators of excitation-contraction coupling in cardiac muscle: Evidence from a novel *CARNS1* knockout rat model

Lívia de Souza Gonçalves [a,f], Lucas Peixoto Sales [a,f], Tiemi Raquel Saito [a,f], Juliane Cruz Campos [b], Alan Lins Fernandes [a,f], José Natali [a], Leonardo Jensen [c], Alexandre Arnold [c], Lisley Ramalho [b], Luiz Roberto Grassmann Bechara [b], Marcos Vinicius Esteca [d], Isis Correa [c], Diogo Sant'Anna [c], Alexandre Ceroni [e], Lisete Compagno Michelini [e], Bruno Gualano [a,f], Walcy Teodoro [f], Victor Henrique Carvalho [g], Bianca Scigliano Vargas [g], Marisa Helena Gennari Medeiros [g], Igor Luchini Baptista [d], Maria Cláudia Irigoyen [c], Craig Sale [h], Julio Cesar Batista Ferreira [b], Guilherme Giannini Artioli [a,f,*]

[a] *Applied Physiology & Nutrition Research Group, School of Physical Education and Sport, Faculdade de Medicina, Divisão de Reumatologia, Universidade de São Paulo, SP, Brazil*
[b] *Institute of Biomedical Sciences, University of Sao Paulo, Brazil*
[c] *Laboratório de Hipertensão do Instituto do Coração do Hospital das Clínicas da Faculdade de Medicina da Universidade de São Paulo, Brazil*
[d] *Laboratory of Cell and Tissue Biology, Faculdade de Ciências Aplicadas, Universidade Estadual de Campinas, Brazil*
[e] *Departamento de Fisiologia, Instituto de Ciências Biomédicas, Universidade de São Paulo, Brazil*
[f] *Rheumatology Division, Faculdade de Medicina FMUSP, Universidade de São Paulo, Brazil*
[g] *Departamento de Bioquímica, Instituto de Química, Universidade de São Paulo, Brazil*
[h] *Musculoskeletal Physiology Research Group, Sport, Health and Performance Enhancement Research Centre, Nottingham Trent University, UK*

ARTICLE INFO

Keywords:
Carnosine
Cardiac dysfunction
Carnosine synthase
Skeletal muscle
Cardiac muscle
Calcium transient

ABSTRACT

Histidine-containing dipeptides (HCDs) are abundantly expressed in striated muscles. Although important properties have been ascribed to HCDs, including H^+ buffering, regulation of Ca^{2+} transients and protection against oxidative stress, it remains unknown whether they play relevant functions *in vivo*. To investigate the *in vivo* roles of HCDs, we developed the first carnosine synthase knockout (CARNS1$^{-/-}$) rat strain to investigate the impact of an absence of HCDs on skeletal and cardiac muscle function. Male wild-type (WT) and knockout rats (4 months-old) were used. Skeletal muscle function was assessed by an exercise tolerance test, contractile function *in situ* and muscle buffering capacity *in vitro*. Cardiac function was assessed *in vivo* by echocardiography and cardiac electrical activity by electrocardiography. Cardiomyocyte contractile function was assessed in isolated cardiomyocytes by measuring sarcomere contractility, along with the determination of Ca^{2+} transient. Markers of oxidative stress, mitochondrial function and expression of proteins were also evaluated in cardiac muscle. Animals were supplemented with carnosine (1.8% in drinking water for 12 weeks) in an attempt to rescue tissue HCDs levels and function. CARNS1$^{-/-}$ resulted in the complete absence of carnosine and anserine, but it did not affect exercise capacity, skeletal muscle force production, fatigability or buffering capacity *in vitro*, indicating that these are not essential for pH regulation and function in skeletal muscle. In cardiac muscle, however, CARNS1$^{-/-}$ resulted in a significant impairment of contractile function, which was confirmed both *in vivo* and *ex vivo* in isolated sarcomeres. Impaired systolic and diastolic dysfunction were accompanied by reduced intracellular Ca^{2+} peaks and slowed Ca^{2+} removal, but not by increased markers of oxidative stress or impaired mitochondrial respiration. No relevant increases in muscle carnosine content were observed after carnosine supplementation. Results show that a primary function of HCDs in cardiac muscle is the regulation of Ca^{2+} handling and excitation-contraction coupling.

* Corresponding author. Applied Physiology & Nutrition Research Group; School of Physical Education and Sport, Faculdade de Medicina, Divisão de Reumatologia, Universidade de São Paulo, Av. Professor Mello Moraes, 65. Cidade Universitaria, Sao Paulo, 05508-030, SP, Brazil.
E-mail address: artioli@usp.br (G.G. Artioli).

https://doi.org/10.1016/j.redox.2021.102016
Received 18 March 2021; Received in revised form 15 May 2021; Accepted 16 May 2021
Available online 20 May 2021

1. Introduction

Histidine-containing dipeptides (HCDs) are abundantly found in skeletal and cardiac muscles, kidneys and brains of humans and other mammals [1]. Carnosine (β-alanyl-L-histidine) and its methylated analogue anserine (β-alanyl-*N*-methylhistidine) are the main HCDs in the skeletal muscle; in the cardiac muscle, acetylated analogues of carnosine (N-Acetyl-L-carnosine) and anserine (N-Acetyl-L-anserine) are also expressed in high amounts [2]. Carnosine is endogenously synthesised by carnosine synthase 1 [3], an enzyme that is encoded by the *CARNS1* gene. Following carnosine formation, other HCDs can be synthesised via carnosine methylation (anserine and ophidine), via carnosine acetylation (N-Acetyl-L-carnosine) or via anserine acetylation (N-Acetyl-L-anserine) [4], although little is currently known about carnosine and anserine acetylation reactions. HCDs are among the most abundant metabolites in striated muscles [5].

Carnosine and its analogues can be obtained from the diet and their endogenous synthesis can be increased via β-alanine supplementation, with the availability of β-alanine being rate-limiting for carnosine synthesis [6]. Although the physiological roles of carnosine have been studied for decades, a definitive conclusion remains elusive. The pK_a of carnosine is 6.83 [7], leading to the assumption that it is a proton (H^+) buffer in skeletal muscle [8]. This is supported by the fact that increased muscle carnosine content increases high- but not low-intensity exercise tolerance [9] and by comparative physiology data [10]. Several other properties ascribed to carnosine might also be physiologically relevant, including protection against oxidative stress [1] and protein glycation [11], detoxification of reactive aldehydes [12] and regulation of Ca^{2+} handling in striated muscles [13,14], suggesting that carnosine is multifunctional and pluripotent. Its exact role(s) in the different tissues where it is located remain unclear, especially as most of the evidence arises from *in vitro* studies. The presence of HCDs in cardiac muscle [5] and in some brain areas [15] suggests other possible roles that are still unknown. The available evidence indicates that carnosine and other HCDs exert diverse, although ultimately beneficial, effects on cellular function. For example, carnosine appears to delay cell senescence and rejuvenate senescent cells *in vitro* [16], whilst at the same time it seems capable of inhibiting the growth of some tumour cells [17], suggesting that the pluripotency of carnosine might have differential tissue-specific functions.

Here, we report the development and characterisation of a novel *CARNS1* gene knockout (*CARNS1*$^{-/-}$) rat strain in which all tissues are devoid of HCDs. This approach enabled us to explore, for the first time, whether the antioxidant, pH-buffering and Ca^{2+} handling properties of carnosine translate into physiologically relevant roles for normal cell and tissue function. An advantage of the rat model is that their normal HCDs content is comparable to that of humans [1], which increases the translational value of the study. Our data reveals that HCDs are key regulators of excitation-contraction (EC) coupling in cardiac, but not in skeletal muscle, opening a new avenue for exploring the therapeutical role of HCDs.

2. Materials and methods

2.1. Development of *CARNS1*$^{-/-}$ rats

CARNS1$^{-/-}$ rats were generated by an outsourced company (Transposagen Inc., USA) with the use of CRISPR-Cas9 technology. Two CRISPR guides (5′-GGCTCAGTGGCTGGCGCTGG and 5′-GGGATTGCTGGAGAAGCTGG) targeting exon 6 of the *CARNS1* gene were injected, along with Cas9 mRNA, into the pronuclei of 46 Wistar rat embryos, four of which were born alive. The resulting mutations were screened by amplicon sequencing and comprised large exonic sequences (>80 bp) that induced frameshift. Three pups showed signs of deletion, with three slightly different alleles being transmitted to the offspring of two founders, thereby confirming germline transmission. All founders were genotyped, and the three expected mutated alleles were confirmed. Because the mutations were similar in their gene locations and sizes, we examined whether they resulted in the same phenotype (i.e., absence of HCDs in striated muscles). Animals carrying two of the three mutated alleles in any combination were considered *CARNS1*$^{-/-}$.

2.2. Animals

Male Wistar *CARNS1*$^{-/-}$ rats and their wild type (WT) controls were housed in groups of 4–5 per cage and were maintained in a controlled environment (temperature 23 ± 2 °C, relative humidity at 55 ± 10%, 12/12 h light/dark cycle) with *ad libitum* access to standard laboratory chow (Nuvilab/Quimtia, Brazil) and filtered water up to their 4th month of age, when they were used for the experiments. All experiments were carried out with the researchers blinded to genotype and were repeated a minimum of 3 times using different groups of animals. The study was approved by the Animal Use Ethics Committee of the University of Sao Paulo (#2014/04) and complied with the normative resolutions (N°. 30–32/2016) of the Brazilian National Council for Animal Experimentation Control (CONCEA).

2.3. Genotyping

Genomic DNA was extracted from the ear clips using the salting-out method and then submitted to PCR reaction (5x buffer; 25 mM $MgCl_2$; 10 μM dNTPmix; 10 μM Primer (forward and reverse); DNA 0,5 μL; Go Taq DNA Polymerase (5u/μL) and Ultrapure water). Thermal cycling conditions were: 2 min 95 °C for 2 min; 35 cycles of 95 °C for 30 s, then 59 °C for 45 s and 72 °C for 1 min; 5 min 72 °C. PCR products were separated in 2% agarose gel electrophoresis and visualised in UV transilluminator.

2.4. Phenotype confirmation

To confirm that *CARNS1*$^{-/-}$ resulted in the absence of HCDs, carnosine and anserine were quantified in duplicate in skeletal muscle using HPLC coupled to UV detection [18], and in cardiac muscle using HPLC coupled to mass spectrometry (ESI + MS/MS) [12]. Approximately 3–4 mg of lyophilised skeletal and cardiac muscles tissues were powdered and deproteinised with 0.5 M $HClO_4$, vortexed for 15 min and centrifuged at 5000 g at 4 °C for 3 min [19]. Samples were neutralised with 2.1 M $KHCO_3$, centrifuged at 5000 g at 4 °C for 3 min, and the supernatant stored at −80 °C for further analysis. Total skeletal muscle HCDs content was determined by HPLC (Lachrom, Merck Hitachi; Tokyo, Japan), as per Mora et al. [18]. All chromatography was conducted at room temperature. Samples and standards were analysed in duplicate and injected via an auto sampler using a cut injection method, with a total aspirated volume of 70 μL; 30 μL was discarded, 10 μL was injected for analysis, and the remaining 30 μL was also discarded. The column used for chromatographic separation was an Atlantis HILIC silica column (4.6 × 150 mm, 3 μm; Waters, Milford, MA) attached to an Atlantis Silica column guard (4.6 × 20 mm, 3 μm). The method used two mobile phases: mobile phase A, 0.65 mM ammonium acetate, in water/acetonitrile (25:75) (v/v), and mobile phase B, 4.55 mM ammonium acetate, in water/acetonitrile (70:30). The pH of both solutions was adjusted to 5.5 using ammonium hydroxide and filtered under vacuum through a 0.2-μm membrane. The separation condition was a linear gradient from 0% to 100% of solvent B in 13 min at a flow rate of 1.4 mL/min. Separation was monitored using an ultraviolet detector at a wavelength of 214 nm. The column was equilibrated for 5 min under the initial conditions before each injection. Quantification was performed using peak areas, which were calculated by computer software coupled to the chromatographer. The peak area for the standard curve was plotted and a regression equation obtained, from which interpolations were used to calculate content. Total cardiac muscle HCDs was determined by on-line HPLC-ESI + -MS/MS was performed as described

before [12] with modifications. The analyses were carried out in the positive mode and detection was conducted on a triple quadrupole mass spectrometer API 6500 (Sciex, Washington D.C, WA), using selected reaction monitoring (SRM). An Agilent HPLC system (Agilent Technologies, Santa Clara, CA) equipped with an autosampler (1200 High performance), a column oven set at 45 °C (1200 G1216B), an automated high pressure flow switching valve, a 1200 Binary Pump SL and a Shimadzu 10-AVp Isocratic Pump (Shimadzu, Tokyo, Japan) were used for sample injection and cleanup on a Kinetex C18 column, with an i.d. of 100 × 4.6 mm and particle diameter of 2.6 μm (Phenomenex, Torrance, CA) followed by a second Kinetex C18 column, with an i.d. of 100 × 2.1 mm and particle diameter 2.6 μm (Phenomenex, Torrance, CA). The mobile phase consisted of 5 mM ammonium acetate pH 5.5 (A) and acetonitrile (B). Prior to use, both solutions were filtered through a 0,22 μm PVDF membrane (Millipore, Bedford, MA). The dipeptide was eluted from the columns according to the following method: from 0 to 4 min, 10% acetonitrile and 150 μL/min; from 4 to 4.1 min flow rate was increased from 150 to 200 μL/min; from 4 to 6 min, 10–25,5% acetonitrile and then increased to 30% acetonitrile from 6 to 10 min. From 10 to 15 min, 30–90% acetonitrile and 200–250 μL/min; from 15 to 20 min, 90% acetonitrile and 90-10% acetonitrile with decrease of the flow rate from 250 to 200 μL/min from 20 to 22 min, followed by equilibration step with decreasing flow rate from 200 to 150 μL/min and 10% acetonitrile until 32min. A high-pressure flow switching valve composed of 2-positions and 6-ports was inserted between the two columns. The valve discarded the eluent from the first column until 3 min of run while kept the second column supplied with a solution of ammonium acetate 5 mM: acetonitrile (9:1, v/v) at a constant flow of 150 μL/min using a Shimadzu 10-AVp Isocratic Pump. After 3 min of run, the valve switched position allowing the eluent from the first column to enter the second column. Upon elution from the second column, the samples were injected into the mass spectrometer. After 18 min of run, the valve switched back to the initial position, allowing both columns to re-equilibrate. Carnosine and anserine were analysed by electrospray ionization (ESI) in the positive mode, and detection was made using selected reaction monitoring (SRM) on a triple quadrupole mass spectrometer API 6500. The Turbo Ionspray Voltage was kept at 5500 V, the curtain gas at 20 psi and the nebulizer and auxiliary gas at 40 psi. The temperature was set to 500 °C, and the pressure of nitrogen in the collision cell was adjusted to medium. The signal to noise ratio (S/N)≥ 7 was used as the quantification criteria. Transitions for anserine: Quantification transition (*m/z*); Confirmation transition (*m/z*) (241 → 170; 241 → 109). Transitions for CAR: Quantification transition (*m/z*); Confirmation transition (*m/z*) (227 → 110; 227 → 156) and $CARd_4$ (231 → 110; 231 → 156) were monitored using a dwell time of 50 ms.

2.5. Body mass, fasting blood glucose and body temperature assessment

Body mass was measured on a digital scale every 30 days, starting from the 30th day of life until the 110th day of life. Blood glucose was measured after a 6-h fast. Three measurements were taken, with an interval of one week. Tail-tip blood samples were collected, and blood glucose was immediately determined using a blood glucose analyser (Accu-chek® Performa, Roche Diagnostics KK, Japan). Core body temperature was measured by inserting a temperature sensor (Inconterm) in the animals' rectum after anaesthesia with isoflurane (2%).

2.6. Direct measurement of blood pressure

Under anaesthesia, an arterial cannula was inserted into the femoral artery and externalised on the animal's back. Twenty-four hours after surgery, arterial cannulas were connected to a pressure transducer, which was coupled to a signal acquisition system (PowerLab System and LabChart 8.0 Software, AD Instruments, Bella Vista, NSW, Australia). Blood Pressure (BP) was measured at a sampling frequency of 2 KHz (2000 samples per second) during 30 min of recording.

2.7. Skeletal muscle morphology

Tibial anterior and soleus muscles were cut in 10 μm cross sections using a cryostat (Leica CM1850, Leica Microsystems, Germany). Histological sections were subjected to hematoxylin and eosin (HE) staining. The images were recorded on a light microscope with 200x magnification.

2.8. Exercise tolerance test

A graded maximal running test was performed on a motorised treadmill. The test started at a speed of 6 m min^{-1}, which was increased by 3 m min^{-1} every 3 min until exhaustion. The test was conducted at 0% inclination and the rats were deemed exhausted when they could no longer maintain speed over 3 min [20].

2.9. In situ skeletal muscle function assessment

Skeletal muscle contractile function was assessed *in situ* using a protocol adapted from Kalmar and Greensmith [21] and MacIntosh, Esau, Holash and Fletcher [22]. Animals were anesthetised with tribromoethanol (20 mg kg/100 g body mass i.p.) and the sciatic nerve was exposed and connected to a platinum electrode. The distal tendon of the *tibialis anterioris* was connected to a surgical silk suture, which was connected to a previously calibrated force transducer. The sciatic nerve was stimulated using an S48 square pulse stimulator (Grass®) and the contractile data were acquired and processed using a data acquisition system (Biopac Systems, USA; AcqKnowledge software, version 4.4). 0.5 V pulses were used to maximise motor unit recruitment. The stimulation protocol consisted of three successive steps separated by 60 s intervals: 1) Single twitch: 5 isolated pulses at 1 Hz, 200 ms duration; 2) Maximum tetanic force: one pulse train at 150 Hz, duration 300 ms; 3) Fatigue test: one pulse train per second at 40 Hz, with the duration of 333 ms for 3 min.

2.10. Muscle buffering capacity ($\beta m_{in\ vitro}$)

Non-bicarbonate buffering capacity of skeletal muscle was determined using the homogenate titration method [23], completed at 37 °C in a dry bath mixer. Approximately 3 mg of freeze-dried muscle was homogenised on ice for 3 min in 10 mM NaF (100 μl for every 3 mg of dry muscle). Homogenate pH was initially adjusted to 7.1 (0.02 M NaOH) and then titrated to a pH of 6.5 by serial addition of 10 mM HCl, with the $\beta m_{in\ vitro}$ being calculated as the amount of H^+ (in millimoles) necessary to change pH from 7.1 to 6.5.

2.11. In vivo echocardiographic assessment of cardiac function

Echocardiograms were performed with the Vevo 2100 Ultrasound System (Visual Sonics, Canada) under anaesthesia with 2% isoflurane. Sonographic structural parameters were determined using M-mode and two-dimensional (B-mode) images. Wall thickness and left ventricular chamber diameter were calculated from linear measurements, and the ejection fraction was calculated by the Teicholz method [24]. Tissue Doppler was measured in the mitral valve annulus with image of the four cardiac chambers to record systolic and diastolic myocardial velocities.

2.12. In vivo electrocardiographic assessment of cardiac electrical activity

Cardiac electrical activity was assessed under anaesthesia (2% isoflurane) with heart rate between 300 and 400 bpm. Electrodes were placed to mimic the DII lead in humans (*i.e.*, negative and positive poles in the thorax at the right and left axillary region, and the ground electrode on the medial face of the left pelvic limb). Cardiac electrical activity was recorded for 10 min (Animal BioAmp/PowerLab System and LabChart 8.0 Software, AD Instruments, Bella Vista, NSW, Australia)

with a sampling rate of 2000 points per second.

2.13. In vitro sarcomere contractile function and Ca^{2+} transient assessment

Left ventricle cardiomyocytes were isolated as described elsewhere [25]. Cardiomyocytes were loaded with Fura-2/AM (1 μM, Thermo Fisher) for 20 min, washed and allowed to rest for a further 40 min. Cardiomyocytes were then stimulated at 0.5 Hz and intracellular Ca^{2+} concentration was measured by fluorescence counting 510 nm emissions after excitation at alternating wavelengths of 340 and 380 nm ($F^{340/380ratio}$). Sarcomere shortening was recorded under the same stimulus by video-based sarcomere spacing acquisition system (SarcLen, IonOptix, Milton, MA, USA). Changes in sarcomere length were recorded and analysed using the IonWizard software (IonOptix, Milton, MA, USA).

2.14. Cardiac muscle morphology

Cardiac muscles were fixed in 10% buffered formalin solution, submitted to paraffin blocking processing and cut in 5 μm cross sections, which were stained with hematoxylin and eosin. The images were recorded on a light microscope (Zeiss LSM510Meta) with 400x magnification, and the micrographs were processed using Image ProPlus 6.0 software (Media Cybernetics).

2.15. Collagen profile area density

Histochemical characterisation of total collagen in cardiac muscle was performed in 5 μm cross-sections with Sirius red staining and analysed under a polarised light optical microscope. Ten histologic fields per slide were used for collagen area analysis, determined by optical density.

2.16. Assessment of cardiac mitochondrial function

Cardiac mitochondria were isolated as described elsewhere [26]. To assess cardiac mitochondrial function, O_2 consumption and hydrogen peroxide (H_2O_2) release were evaluated in isolated mitochondria [27]. O_2 consumption was monitored using a computer-interfaced Clark-type electrode (OROBOROS, Oxygraph-2k) and H_2O_2 was measured by spectrofluorimetry (F-2500 Hitachi). Both experiments were performed in 0.25 mg of isolated cardiac mitochondria in 2 ml of experimental buffer (125 mM sucrose, 65 mM KCl, 10 mM Hepes, 2 mM inorganic phosphate, 2 mM $MgCl_2$, 100 μM EGTA, and 0.01% BSA, pH 7.2) containing succinate, malate, and glutamate substrates (2 mM of each) with continuous stirring at 37 °C. To estimate O_2 consumption and H_2O_2 release during State 3 and State 4 respiratory rates, and in uncoupled mitochondria, we added ADP (1 mM, Amresco), oligomycin (1 μg ml^{-1}, Sigma-Aldrich) and FCCP (0.1 mM). The Amplex Red (25 μM)-horseradish peroxidase (0.5 U $ml.^{-1}$, Sigma-Aldrich) system was used to measure H_2O_2 release (λex = 563/λem = 587 nm). Calibration was conducted by adding H_2O_2 at known concentrations (A240 = 43.6 M^{-1} cm^{-1}) to the experimental buffer.

2.17. Assessment of protein carbonyl in cardiac muscle

Protein carbonylation was determined using a DNPH (2,4-dinitrophenylhydrazine)-based colorimetric assay kit (ab126287 - Abcam) following manufacturer's recommendations.

2.18. Immunoblotting

Tissue samples were homogenised in 30 vol of extraction buffer (0.625% Nonidet P-40, 0.625% sodium deoxycholate, 6.25 mM sodium phosphate pH 7.2, 1 mM EDTA pH 8.0, 1% phosphatase and protease inhibitor cocktails). Total protein was quantified in the supernatant using the Bradford protein assay and 20–40 μg of protein was loaded into polyacrylamide gel for electrophoresis. SERCA2 was separated in a 12% gel while Phospholamban was separated in a 4–20% gradient precast gel (Mini-PROTEAN® TGX™, BioRad). After separation, proteins were transferred to a nitrocellulose membrane using a transfer buffer containing 10% methanol. Membranes were then blocked with 5% skim milk and incubated overnight with the primary antibody diluted in 5% BSA in the following concentrations: *anti*-Serca2 (ab3625, 1:1000), *anti*-Phospolamban (Abcam, ab85146, 1:1000), *anti*-Phospolamban-Phospo (ab62170, 1:1000). Membranes were then incubated with secondary antibodies conjugated with peroxidase (goat anti-rabbit polyclonal, Jackson ImmunoResearch 111–035003; 1:10000) for 1 h. Protein bands were visualised using ECL Western Blotting Substrate (32106) in a Syngene G:BOX image acquirer.

2.19. Real-time RT-PCR

The expression of *PHT1* and *PHT2* genes (encoding carnosine transporting proteins) was assessed in left ventricles via real-time RT-PCR. Total RNA was isolated using Trizol® (Invitrogen) and chloroform and precipitated in isopropanol. RNA concentration and purity were measured in a micro-spectrophotometer (NanoDrop ND2000, Thermo Scientific), with integrity being confirmed in denaturing agarose gel. cDNA was synthesised with oligo DT and M-MLV reverse transcriptase (Promega). PCR was carried out with 20 ng cDNA, 22 μl SYBR™ Green (Applied Biosystems) and 300 nM of each primer in a final volume of 44 μl. The cycling conditions were: 50 °C for 2 min, 95 °C for 10 min, 40 cycles of 95 °C for 15 s and 60° for 60 s, and a final 65-95 °C melting ramp with 1 °C increments. Signal intensity was monitored using the Rotor Gene-Q HRM system (Qiagen). Relative gene expression was calculated using the $2^{-\Delta\Delta Ct}$ method with the *YWHAZ* gene being used as the reference gene. Primers sequences were as follows: PHT1 5′-GAGGGCCGTTCACAGAGGA-3′ and 5′-TGAGGCCTTATAGTCTGCAG-3'; PHT2 5′- GAGTCTGGGTCACGGAGAC-3′ and 5′- GAGGCCCACGATGATGCTG-3'.

2.20. Data analysis

Data are presented as mean ± SD. Body mass and force production in the fatigue test were analysed with mixed models (proc mixed, SAS v. 9.4). *Post-hoc* tests, corrected for multiple comparisons with the Tukey-Kraemer adjustment, were used to locate significant differences whenever significant main effects or interaction effects were shown. The distribution of total collagen area was compared between genotypes using the Kolmogorov-Smirnov test (RStudio v.4.0.0). For all other variables, Welch's two-sample t-tests for unequal sample sizes were used to compare *CARNS1*$^{-/-}$ *vs.* WT (RStudio v.4.0.0). Effect sizes (ES) were calculated using Cohen's d ($Mean_1$ - $Mean_2$)/SD_{pooled}) when sample number between the groups was similar, and when different, the Hedges' g correction was used (1–3/4(n-9) [28].

3. Results

3.1. *CARNS1*$^{-/-}$ lead to complete HCDs depletion in striated muscles

CARNS1$^{-/-}$ rats were generated by Transposagen Inc. (USA) using the CRISPR-Cas9 technology to induce large intronic mutations (>80 bp) resulting in frameshift (Fig. 1A–B). In our laboratory, they were genotyped and bred to homozygosity. *CARNS1*$^{-/-}$ genotype resulted in the absence of HCDs in skeletal (Fig. 1C–D) and cardiac (Fig. 1E and F) muscles. The complete absence of HCDs resulted in viable animals, demonstrating that HCDs are not essential to life. These results also indicate that our model is suitable to investigate the impact of an absence of carnosine and other HCDs on striated muscle homeostasis *in vivo*.

3.2. *CARNS1*$^{-/-}$ resulted in an apparently normal phenotype

Visual inspection showed no impact of the absence of HCDs on gross phenotype (Fig. 2A). Likewise, histological analyses of skeletal and cardiac muscles showed preserved morphological characteristics (Fig. 2B). *CARNS1*$^{-/-}$ did not affect fertility, as assessed by the number of viable pups per mating (Fig. 2C), nor did it affect somatic growth (Fig. 2D), or body temperature (Fig. 2E). No differences in cardiac and skeletal muscle mass were shown between genotypes (Fig. 2F and G). Evidence from cultured cells suggests that carnosine might increase glucose uptake by skeletal muscle [29]. We thus explored whether glucose metabolism would be impacted by *CARNS1*$^{-/-}$, but we showed no effect of an absence of HCDs on occasional glycaemia (Fig. 2H); as such, no further effects on glucose metabolism were examined.

3.3. *CARNS1*$^{-/-}$ did not affect exercise capacity and muscle buffering capacity

Increased intramuscular carnosine improves high-intensity exercise capacity, likely due to its H^+ buffering effect [30] and possibly due to improved force-generation in response to augmented Ca^{2+} sensitivity [31]. To test whether the absence of HCDs results in impaired exercise tolerance, animals were submitted to a progressive maximal exercise test on a treadmill. Contrary to our hypothesis, exercise tolerance was similar between *CARNS1*$^{-/-}$ and their WT controls (Fig. 2I), suggesting that the absence of HCDs does not affect muscle buffering capacity or

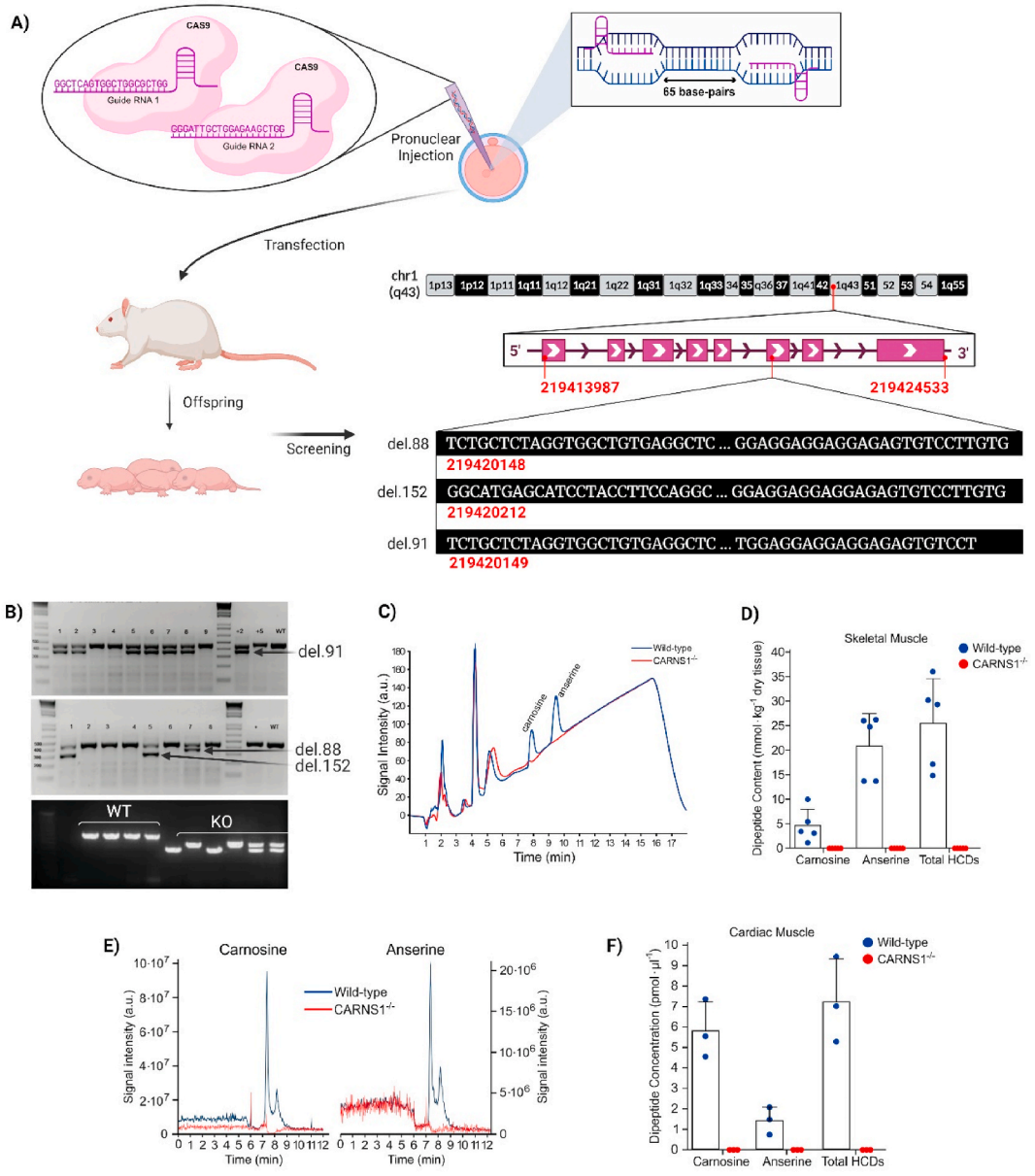

Fig. 1. A) Two CRISPR guides were designed targeting exon 6 of the *CARNS1* gene aiming at large deletions and frameshift. They were injected along with Cas9 into pronuclei of rat embryos. **B)** Offspring were screened via gene sequencing and 3 mutated alleles were identified. The red numbers display their chromosome positions, the DNA sequences in white display their deleted sequences, along with the size of the deletions. PCR genotyping confirmed amplicon sizes (upper gel images were carried out at Transposagen Inc.). In-house genotyping of rats bred to homozygosity confirmed transmission of mutated alleles. **C and D)** Representative chromatograms and HCD quantification via HPLC in skeletal muscle samples of WT and *CARNS1*$^{-/-}$ rats. Signals below the limits of detection were deemed zero. **E and F)** Representative SRM chromatograms and histidine-containing dipeptide quantification via HPLC-ESI + -MS/MS in cardiac muscle samples in WT and *CARNS1*$^{-/-}$ rats. The signal to noise ratio of ≥3 was used as the detection criteria for the adducts and a S/N ≥ 7 was used as the quantification criteria. Values below this threshold were deemed zero. (For interpretation of the references to color in this figure legend, the reader is referred to the Web version of this article.)

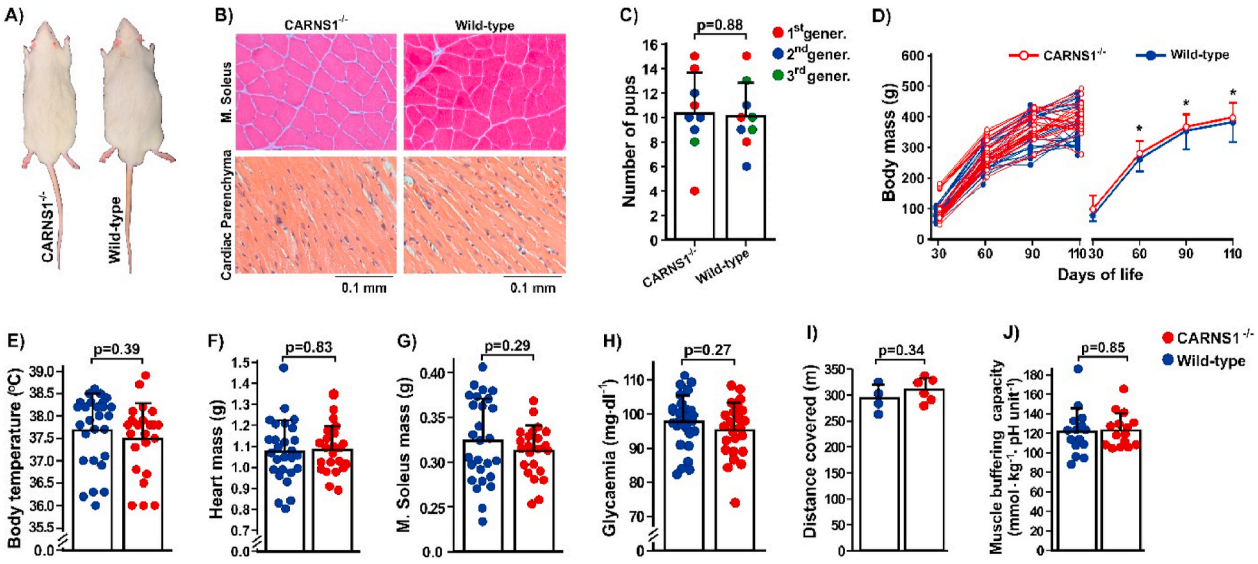

Fig. 2. A) Representative photograph of 4-month-old *CARNS1*$^{-/-}$ and WT rats showing no apparent phenotypic difference between genotypes. **B)** Representative hematoxylin and eosin-stained histological slides of skeletal (*m. soleus*) and cardiac muscle depicting normal tissue morphology. **C)** Number of pups per mating couple during three generations, indicating that the absence of HCDs does not affect fertility. **D)** Body mass was similar between genotypes (WT: n = 28; *CARNS1*$^{-/-}$: n = 28). Mixed models: main effect of time: F(3, 50.4) = 1276.56, p < 0.0001; main effect of genotype: F(1, 55.1) = 2.57, p = 0.11; genotype*time interaction: F(3, 50.4) = 0.23, p = 0.88. *p < 0.05 *vs.* the previous time point (within-group effects). **E-H)** Physiological parameters (rectal temperature: WT n = 16, CARNS1$^{-/-}$ n = 17; heart mass: WT n = 27, CARNS1$^{-/-}$ n = 23; m. soleus mass: WT n = 27, CARNS1$^{-/-}$ n = 23; occasional glycaemia: WT n = 16, CARNS1$^{-/-}$ n = 17) were similar between genotypes. **I)** Distance covered in a progressive maximal running test (WT: n = 4, CARNS1$^{-/-}$: n = 6). **J)** The *in vitro* determined muscle buffering capacity (WT: n = 15, CARNS1$^{-/-}$: n = 15; ES: −0.04).

muscle function.

We next determined the *in vitro* buffering capacity of skeletal muscle extracts, which confirmed the lack of effect of the absence of HCDs on muscle buffering capacity (Fig. 2J). In addition to the putative role of carnosine on skeletal muscle pH-regulation, it has been shown that carnosine induces a rapid Ca^{2+} release from the sarcoplasmic reticulum [13], and increases the sensitivity of Ca^{2+}-channels [13] and the contractile apparatus to Ca^{2+} [31]. Indirect evidence from human studies has also suggested that carnosine could potentiate Ca^{2+} reuptake to the sarcoplasmic reticulum [32]. We thus investigated whether the absence of HCDs affects force generation, contractile properties and tolerance to fatigue via *in situ* electrical stimulation of the sciatic nerve.

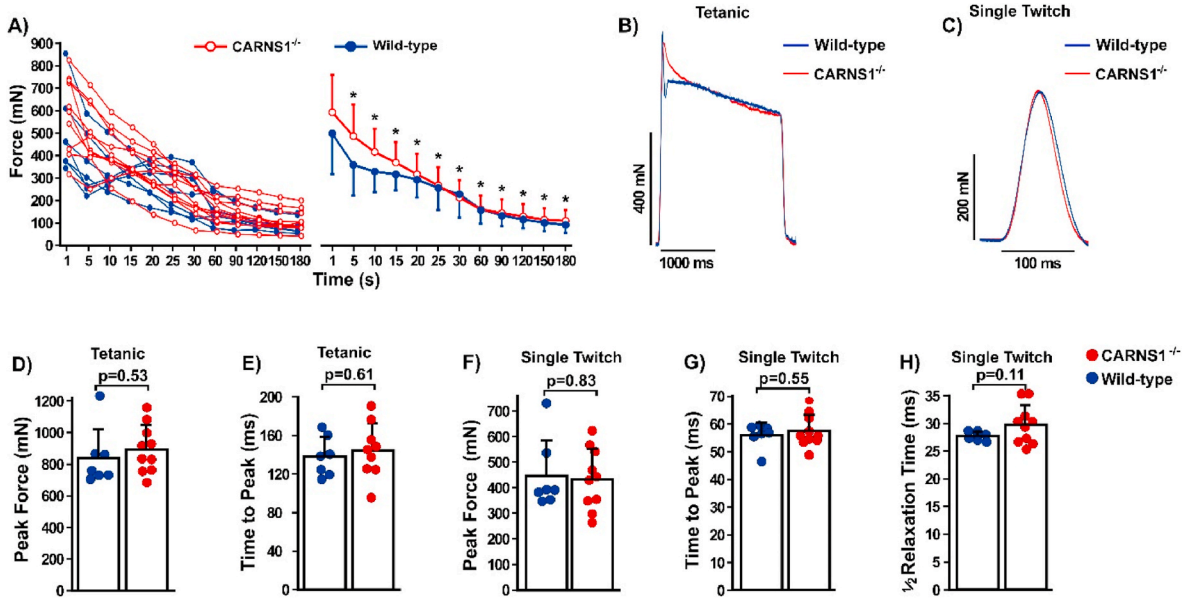

Fig. 3. A) Individual and mean-group electrically-evoked force responses to a 3-min fatigue protocol (WT: n = 7, CARNS1$^{-/-}$: n = 10). No significant differences were shown between genotypes. (Mixed models: main effect of time: F (7, 9) = 38.21, p < 0.0001; main effect of genotype: F(1, 15) = 0.84, p = 0.37; genotype*time interaction: F(7, 9) = 1.15, p = 0.41. *p < 0.05 *vs.* the previous time point (within-group effects). **B and C)** Representative electrically-evoked maximal tetanic and single twitch contractions showing the similarities between WT and CARNS1$^{-/-}$ rats. **D and E)** Peak force (ES: −0.31) and time to peak (ES: −0.24) during electrically-evoked maximal tetanic contraction (WT: n = 7, CARNS1$^{-/-}$: n = 10). **F–H)** Peak force (ES: −0.10), time to peak (ES: −0.27) and half-relaxation (ES: −0.68) time during electrically-evoked single twitch contraction (WT: n = 7, CARNS1$^{-/-}$: n = 10). All p-values displayed in the dot plots refer to Welch two-sample t-tests.

3.4. *CARNS1*$^{-/-}$ did not affect skeletal muscle contractility

The absence of HCDs did not impact muscle resistance to fatigue (Fig. 3A), corroborating the absence of changes in exercise tolerance, H^+ buffering and muscle function. Since intramuscular acidosis can play a major causative role in fatigue [33], our data provide novel evidence that HCDs might not be essential for intramuscular pH regulation. Moreover, peak force attained in both single twitch and maximal tetanic contractions, as well as time to peak force and half-relaxation time were also similar between *CARNS*$^{-/-}$ and WT animals (Fig. 3B–H). Since the contraction-relaxation cycle in skeletal muscle is mainly dependent upon Ca^{2+} transients [34], these findings suggest that HCDs are not essential for Ca^{2+} handling, at least in the skeletal muscle under normal conditions.

3.5. *CARNS1*$^{-/-}$ resulted in abnormal cardiac function

We next assessed *in vivo* cardiac function using echocardiography, which showed evidence of impaired function (Fig. 4A). Specifically, *CARNS1*$^{-/-}$ rats displayed increased isovolumetric contraction time

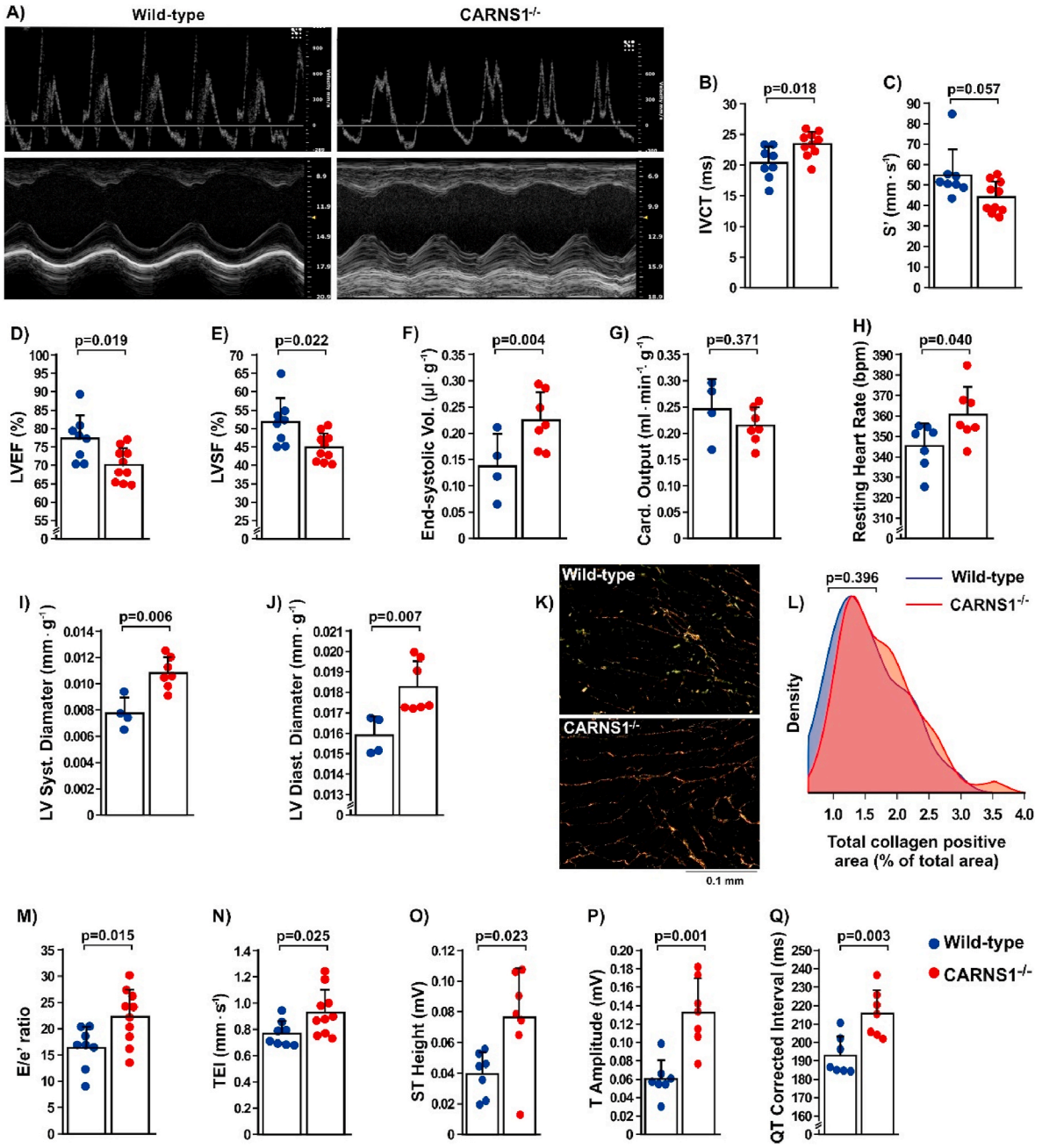

Fig. 4. A) Representative images of B- and M-mode *in vivo* echocardiographic assessment of cardiac function in *CARNS1*$^{-/-}$ rats and WT controls. **B-G)** Isovolumetric contraction time (IVCT - ES: −1.26), systolic perfusion velocity (S'- ES: 1.01), left ventricle ejection fraction (LVEF % - ES: 1.27) and left ventricle shortening fraction (% LVSF – ES: 1.28) (WT: n = 8, *CARNS1*$^{-/-}$: n = 10), end systolic volume and cardiac output adjusted by body mass (WT: n = 4, *CARNS1*$^{-/-}$: n = 7; ES: −1.42). **H-J)** Resting heart rate measured during electrocardiogram (WT: n = 7, *CARNS1*$^{-/-}$: n = 7; ES: −1.16), left ventricular systolic and diastolic diameter adjusted by body mass (WT: n = 4, *CARNS1*$^{-/-}$: n = 7; ES: −2.32 and −1.86, respectively). **K-L)** Representative images of total collagen positive signal in the cardiac tissue and density plot of total collagen quantification in the WT (n = 5) and *CARNS1*$^{-/-}$ (n = 5) groups (Kolmogorov-Smirnov test for between-genotype differences in distributions – ES: −0.03). **M-N)** E/e' ratio (ES: −1.20) and cardiac performance index (TEI - ES: −1.06) (WT: n = 8, *CARNS1*$^{-/-}$: n = 10); **O-Q)** ST-wave amplitude (ES: −1.39), T-wave amplitude (ES: −2.26) and QTc interval (ES: −1.83), (WT: n = 7, *CARNS1*$^{-/-}$: n = 7). All p-values displayed in the dot plots refer to Welch two-sample t-tests.

(IVCT, Fig. 4B), suggestive of impaired systolic function [35]. A near-significant reduction ($p = 0.057$) in peak systolic annular velocity (S', Fig. 4C), as well as significant reductions in left ventricle ejection fraction (LVEF, Fig. 4D) and left ventricle shortening fraction (LVSF, Fig. 4E) were shown in the *CARNS1*$^{-/-}$ rats. These results indicate that the absence of HCDs leads to impaired systolic function that is translated into greater difficulty of the left ventricle to pump blood out, thereby increasing the end-systolic.

Despite the reduced systolic function, resting cardiac output was preserved in the *CARNS1*$^{-/-}$ rats (Fig. 4G), indicating a compensation for reduced ejection volume via increased chronotropism (Fig. 4H). The preserved cardiac output is in agreement with the lack of changes in exercise tolerance during the maximal running test. *CARNS1*$^{-/-}$ rats exhibited a loss in compliance and elastic recoil in the left ventricle, as indicated by the lower ejection fraction and higher end systolic volume. This was confirmed by a change in geometry of the left ventricle, shown by an increased cavity diameter during systole and diastole (Fig. 4I and J). To investigate whether these changes in geometry were linked with increased cardiac fibrosis, we assessed total collagen in cardiac tissue, which showed comparable content in *CARNS1*$^{-/-}$ rats in comparison with WT (Fig. 4K and L). Other echocardiographic parameters are displayed in Supplementary Table 1.

The *in vivo* assessment of cardiac function showed not only systolic dysfunction, but also the onset of diastolic dysfunction in the *CARNS1*$^{-/-}$ rats, as they showed a significant reduction in the e' wave (supplementary Table 1) and a higher E/e' ratio (Fig. 4M), indicating abnormalities in left ventricle relaxation, despite apparently normal E-A waves ratios (E/A) (supplementary Table 1). The cardiac performance index (TEI index) of the *CARNS1*$^{-/-}$ rats was higher than WT (Fig. 4N), demonstrating that global ventricular function was impaired due to the overload imposed on the myocardium [36].

3.6. Knockout of the CARNS1 gene resulted in abnormal electrical activity in cardiac muscle

Using electrocardiography, we next investigated whether systolic and diastolic dysfunction were linked to impaired electrical activity of the heart. This showed significant ST-segment elevation (Fig. 4O), suggesting an abnormality in phase 2 of the action potential (plateau), during which Ca^{2+} channels are opened. This corroborates the echocardiographic data showing impaired systolic function and suggests that the underlying mechanism could be related to impaired Ca^{2+} handling. *CARNS1*$^{-/-}$ rats exhibited higher T-wave amplitudes (Fig. 4P), indicating an impairment in the repolarisation phase and a possible delay in Ca^{2+} reuptake during diastole, and longer corrected QT intervals (Fig. 4Q).

3.7. Knockout of the CARNS1 gene resulted in impaired sarcomere contractility and Ca^{2+} transients in isolated adult cardiomyocytes

We next conducted *ex vivo* experiments in isolated adult cardiomyocytes to confirm the impairment of contractile function and further investigate the involvement of Ca^{2+} handling on the described functional changes. *CARNS1*$^{-/-}$ rats showed a significant reduction in sarcomere shortening (Fig. 5A–B), maximal shortening (+dL/dt, Fig. 5C) and re-lengthening (-dL/dt, Fig. 5D) velocities, and an increased time to achieve 50% of maximal shortening (Fig. 5E) and 50% of maximal re-lengthening (Fig. 5F). Since our *in vivo* and *ex vivo* functional data pointed to a possible impairment in Ca^{2+} handling in the *CARNS1*$^{-/-}$ rats, we then directly examined Ca^{2+} transients in isolated cardiomyocytes. Our Ca^{2+} transient analyses showed that Ca^{2+}amplitude was lower in *CARNS1*$^{-/-}$ rats (Fig. 5G and H), with no differences between genotypes shown for basal Ca^{2+} and time to reach 50% of Ca^{2+} peak (Fig. 5I and J). The time to reach 50% of Ca^{2+} decay was increased (Fig. 5K), indicating that Ca^{2+} removal rates were reduced in *CARNS1*$^{-/-}$ rats. These findings align with early *in vitro* data indicating that carnosine has a Ca^{2+} activation property (Lamont and Miller, 1992), probably acting as an EC coupling Ca^{2+} regulator in the cardiac muscle. To further understand whether these changes could be linked to altered protein expression, we assessed Ca^{2+} handling protein expression and post-translational modifications via Western Blotting, which showed no differences between genotypes in SERCA2, total Phospholamban, phosphorylated Phospholamban$^{S16+T17}$ expression and the total/phosphorylated ratio (Fig. 5L and 5M).

3.8. No evidence of increased oxidative stress and impaired mitochondrial function in the *CARNS1*$^{-/-}$ rat cardiomyocytes

A purported function of carnosine is to serve as part of the non-enzymatic antioxidant defence [1]. Since increased ROS production and oxidative stress can lead to mitochondrial dysfunction [37], we assessed mitochondrial function in cardiomyocytes. Our results showed that O_2 consumption and H_2O_2 release by mitochondria were not different between genotypes (Fig. 5N, O and P). The preserved mitochondrial function in the *CARNS1*$^{-/-}$ rats suggests that HCDs do not play a relevant antioxidant role in cardiomyocytes under physiological conditions.

Carnosine can bind to carbonyl groups and prevent cross-linking with proteins [38], with this being a major antioxidant mechanism of carnosine. To further explore whether this property translates into a physiologically relevant function, we determined protein carbonyl levels in cardiac tissue. No differences between genotypes were shown (Fig. 5Q), suggesting that HCDs are not essential for the defence against protein carbonylation, as previously suggested to be the case in skeletal muscle [10]. These data suggest that the absence of HCDs does not result in increased oxidative stress in cardiac tissue, and that the cellular mechanisms underpinning cardiac dysfunction shown in the *CARNS1*$^{-/-}$ rats do not involve increased oxidative stress or impaired mitochondrial respiration.

3.9. Carnosine supplementation to rescue tissue HCDs levels and function

To test whether carnosine supplementation could rescue tissue carnosine levels and further explore the link between HCDs and the alterations shown in the previous experiments, four 4-month old female *CARNS1*$^{-/-}$ rats were supplemented with carnosine (1.8% in drinking water) for 12 weeks – a protocol that has been shown to induce large increases in intramuscular carnosine [39], and four male WT controls without supplementation were used as a reference for normal physiological carnosine levels. Carnosine was determined in the *tibialis anterioris* using HPLC/ESI^{+}MS/MS. Despite the long supplementation period, no relevant increases in muscle carnosine content were observed (supplemented CARNS1$^{-/-}$ rats: 0.08 ± 0.07 mmol kg^{-1} DM, range: 0.04–0.18 mmol kg^{-1} DM; WT controls: 12.1 ± 5.1 mmol kg^{-1} DM, range: 8.8–19.6 mmol kg^{-1} DM). Since we were unable to raise tissue carnosine to near-physiological levels, it was not possible to conduct any further rescue-of-function experiments in the *CARNS1*$^{-/-}$ rat model. To get further insight on why carnosine supplementation did not lead to increments in tissue carnosine, we evaluated the expression levels of the genes encoding PHT1 and PHT2, two proton-coupled oligopeptide transporters that might transport carnosine into tissues [1] and were previously shown to be expressed in skeletal and cardiac muscles [40]. A relatively low expression of these two genes (*vs.* constitutively expressed genes) was shown in the cardiac muscle, with no significant differences being shown between genotypes (supplemental Fig. 1).

4. Discussion

Our novel approach to study the role of HCDs to normal function shows that HCDs are important regulators of EC coupling in cardiac muscle, where it enhances Ca^{2+} amplitude during contraction and speeds up Ca^{2+} reuptake during relaxation. Our findings show that

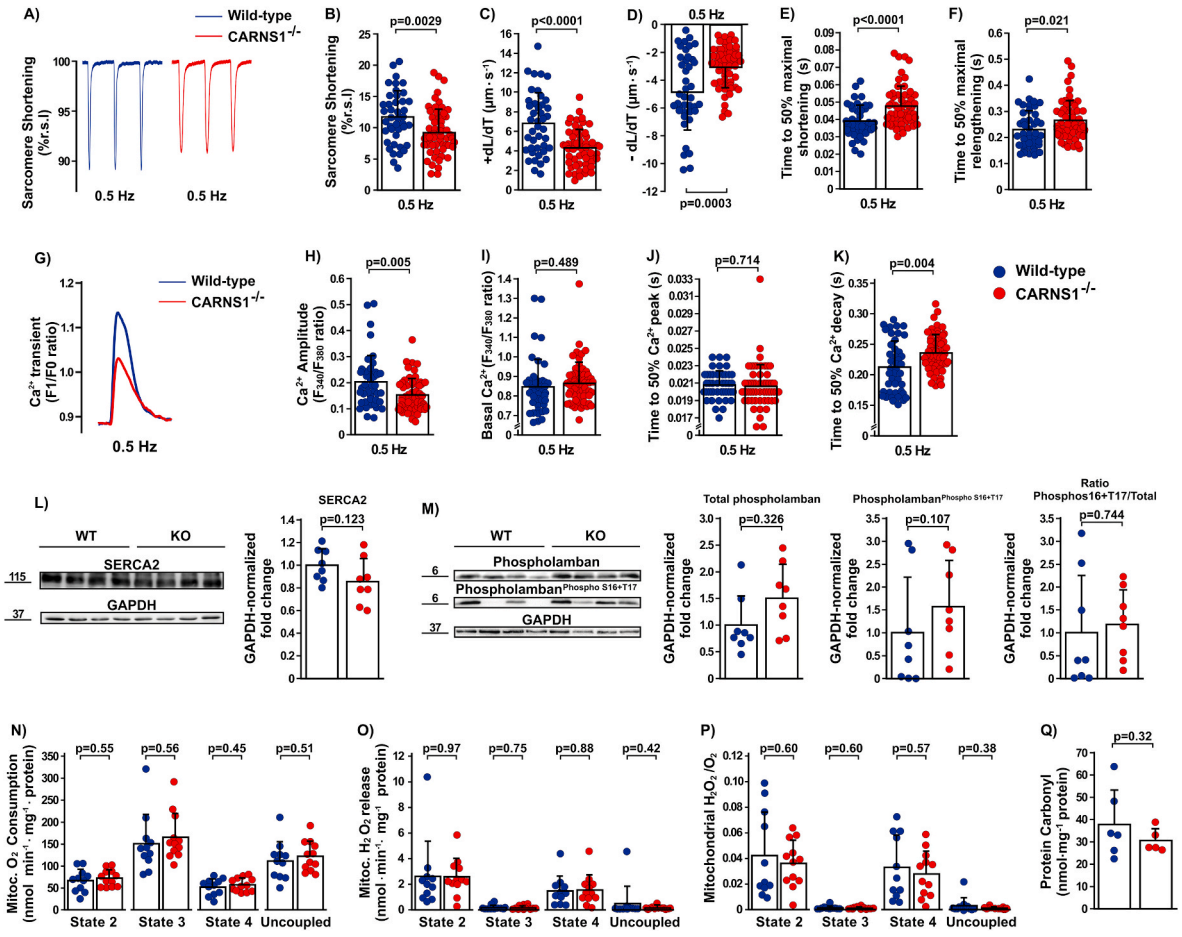

Fig. 5. A–B) Representative traces and analysis of sarcomere shortening (%r.s.l, resting sarcomere length) (ES: −0.004) (WT: n = 43 cells from 3 rats; *CARNS1*$^{-/-}$: 57 cells from 3 rats). **C–F)** Maximal shortening velocity (+dL/Dt - ES: 0.35), maximal relengthening velocity (-dL/dT- ES: −0.22) (WT: n = 42 cells from 3 rats; *CARNS1*$^{-/-}$: 57 cells from 3 rats), time to 50% of maximal shortening (ES: −0.002) (WT: n = 43 cells from 3 rats; *CARNS1*$^{-/-}$: n = 56 cells from 3 rats), and time to 50% of maximal relengthening (ES: −0.001) (WT: n = 43 cells of 3 rats; *CARNS1*$^{-/-}$: n = 56 cells from 3 rats). **G-K)** Representative traces of Ca^{2+} transient, Ca^{2+}amplitude, Basal Ca^{2+}, time to 50% of Ca^{2+} peak (WT: n = 43 cells from 3 rats; *CARNS1*$^{-/-}$: 57 cells from 3 rats), and time to 50% of Ca^{2+} decay (WT: n = 43 cells from 3 rats; *CARNS1*$^{-/-}$: 56 cells from 3 rats). **L-M)** Representative immunoblottings (numbers beside blots represent molecular weight in kDa) and their respective GAPDH-normalised density quantification showing protein expression levels in the cardiac tissue (WT: n = 8; *CARNS1*$^{-/-}$: n = 8); ES: SERCA2 (0.78), total Phospholamban (−0.81) and Phospholamban$^{S16+T17}$ (−0.48). **N–P)** Mitochondrial O_2 consumption, mitochondrial H_2O_2 release and mitochondrial H_2O_2/O_2 ratio in isolated mitochondria from left ventricle (WT: n = 11; *CARNS1*$^{-/-}$: n = 12; ES: all <0.26). **Q)** Carbonylated protein concentration in the cardiac muscle lysate (WT: n = 6; *CARNS1*$^{-/-}$: n = 5; ES: 0.40). All p-values displayed in the dot plots refer to Welch two-sample t-tests.

carnosine, and its methylated analogues, may have potential therapeutic roles, especially for cardiac function, expanding recent evidence indicating that increased carnosine can protect the heart against ischemia-reperfusion injury [41].

As expected, knockout of the *CARNS1* gene resulted in the complete absence of carnosine and anserine in striated muscles, which indicates that carnosine synthase is the sole route for intramuscular synthesis of carnosine, and that anserine synthesis can only occur if carnosine is available. Although not measured in this study, the acetylated analogues of carnosine and anserine are also thought to be lacking in our model, as they seem to be synthesised from carnosine [1], and thus would require the presence of carnosine to be formed. Absence of HCDs did not result in embryonic lethality or any other apparent phenotypic abnormality, indicating that HCDs do not seem to be essential to life, but instead have specialised functions relevant to normal cell function, and essential to cardiac cell function.

The pKa of carnosine is 6.83 [7], making it a H^+ buffer across the physiological pH transit range in skeletal muscle. Unexpectedly, we did not show any evidence to support a H^+ buffering role, since *CARNS1*$^{-/-}$ animals showed no loss of exercise capacity, muscle contractile function or any increase in fatigability in a highly glycolytic muscle (*i.e.*, *tibialis anterioris*). Moreover, there was no evidence of reduced *in vitro* muscle buffering capacity in the *CARNS1*$^{-/-}$ rats. Our data does not, however, imply that carnosine is not a H^+ buffer in skeletal muscle, but rather indicates that carnosine is not essential to support normal buffering capacity and skeletal muscle function. The contribution of carnosine to the total muscle buffering capacity is estimated to be ~10% [6], which seems to be entirely compensated for when carnosine is absent. Although our data indicated that skeletal muscle function is not reliant upon HCDs, we cannot rule out that it plays specialised roles when present. Increased muscle carnosine has been associated with improved detoxification of reactive aldehydes via adduct formation [12]. Interestingly, a role for carnosine in H^+ buffering and aldehyde detoxification was shown recently in cardiomyocytes under low intracellular pH following ischemia in experimental models where carnosine was increased above physiological levels [41]. This suggests that, although carnosine may not exert a specific function under normal physiological conditions, it may offer protection under stressful conditions that challenge cellular function and survival.

The rather similar contractile properties between *CARNS1*$^{-/-}$ and WT controls points to the lack of an effect of HCDs on Ca^{2+} handling in skeletal muscle. Our data disagrees with *in vitro* studies showing that

carnosine increases sensitivity of the contractile apparatus and Ca^{2+} channels to calcium, which was associated with increased force responses in the presence of carnosine [13,31]. Our findings are, however, in alignment with *in vivo* whole-body studies showing no effect of increased carnosine on muscle function [32]. Although our data do not refute the Ca^{2+} sensitising properties of carnosine, it indeed indicates that this function is not relevant for skeletal muscle contraction. Interestingly though, our data show that carnosine does play a fundamental role in the regulation of Ca^{2+} handling in cardiac muscle cells, with a profound impact upon EC coupling and cardiac function.

The crucial role of Ca^{2+} in EC coupling of striated muscles is well established [42]. Skeletal and cardiac muscle cell contraction involves sarcolemma depolarisation and opening of L-type Ca^{2+} channels, leading ryanodine receptors (RYRs) to release Ca^{2+} from the sarcoplasmic reticulum, resulting in Ca^{2+} spark, cross bridge formation and sarcomere shortening [42]. Cell relaxation is then initiated with Ca^{2+} being taken back up by the sarcoplasmic reticulum, through the action of sarcoplasmic/endoplasmic reticulum calcium ATPase (SERCA) pumps, and to the mitochondria, through the action of mitochondrial calcium uniporters. Ca^{2+} can be also extruded to the extracellular medium through sodium-calcium exchangers [42]. Although the mechanism underlying the differential impact of HCDs absence between skeletal and cardiac muscles remains unclear, we can speculate that it might be linked to differences in structure and function between the isoforms of Ca^{2+} handling proteins expressed in the skeletal and in cardiac muscles. L-type channel-mediated Ca^{2+} influx is not relevant for skeletal muscle contractility, as there is a physical interaction between L-type Ca^{2+} and RyR1 channels that is capable of opening the sarcoplasmic reticulum [43]. In the cardiac muscle, however, the interaction between L-type Ca^{2+} and RYR2 channels is indirect and seems to involve Ca^{2+} as a signal transmitter [44]. The reduction in Ca^{2+} amplitude showed in the *CARNS1*$^{-/-}$ rats seems to suggest that HCDs are important physiological regulators of the interaction between L-type Ca^{2+} and RYR2 channels in the cardiomyocyte. This is further supported by a previous *in vitro* study in skinned cardiac cells, which showed that carnosine may regulate RYR2 opening [45]. In addition, under low Ca^{2+} conditions, the sensitisation of contractile proteins to Ca^{2+} is lower in the cardiac muscle than in the skeletal muscle [46], reinforcing our findings that HCDs can be essential to myofilament cross-bridge formation and mechanical force development in the cardiac muscle only.

Our data showed a slower rate of Ca^{2+} removal from the cytoplasm in cardiomyocytes and a slower sarcomere re-lenghtening in *CARNS1*$^{-/-}$ rats, demonstrating that HCDs are also involved in cardiac cell relaxation. While these effects cannot be accounted for by altered SERCA2 expression or Phospholamban-mediated SERCA2 activity, one may speculate that HCDs interact with SERCA2 in the cardiomyocyte to regulate SERCA2 activity or the affinity between SERCA2 and Ca^{2+}. In addition, previous studies in resting isolated cardiac myocytes showed that Ca^{2+} can be transported across the cytosol in a H^+-coupled manner, a mechanism mediated by diffusible H^+ and Ca^{2+} buffers, such as carnosine and other HCDs [47]. Acidic microdomains generate a flux of unprotonated HCDs bond to Ca^{2+}, which serve as Ca^{2+} pumps into these local cytosolic pockets of increased H^+; there, the HCDs buffer the release of Ca^{2+} and become protonated. Because excitation and contraction are activated by Ca^{2+}, this mechanism seems to be important for normal cardiac cell function [47] and it could account for the impaired contractile function shown in our HCDs-absent *CARNS1*$^{-/-}$ rats. Future studies should investigate how HCDs affect SERCA2 or RyR2 activity to unravel the mechanistic basis underpinning the regulatory role of HCDs on calcium transients in the cardiomyocyte.

Since increased oxidative stress is linked with impaired mitochondrial respiration, increased peroxide production and cardiac dysfunction [37], we sought to confirm whether the putative antioxidant role of carnosine would be linked with the cardiac dysfunction shown in *CARNS1*$^{-/-}$ rats. In contrast to *in vitro* studies showing that carnosine can interact with reactive oxygen species and prevent damage to the lipid components of cell membranes [48,49], our data indicate that HCDs are not relevant for primary intracellular antioxidant defence, at least in cardiac muscle under normal resting conditions. This also suggests that the only clear causal link between HCDs and reduced cardiac function shown herein is impaired Ca^{2+} handling. Whilst HCDs, and especially carnosine, seem to be protective under conditions of exacerbated oxidative stress [41], our data indicate that acting as an antioxidant is not a primary physiological role of HCDs in the cardiac muscle.

A rescue-of-function experiment could provide additional evidence that the functional alterations reported in the CARNS1$^{-/-}$ are indeed linked with the absence of HCDs. This led us to conduct a 3-month carnosine supplementation experiment to initially test whether intramuscular carnosine could be restored to near-physiological levels in our knockout model. This supplementation protocol is 3 times longer than that used by Everaert et al. [39], who showed a >160% increase in muscle carnosine content. Tissue carnosine could be increased either by *1)* the uptake of β-alanine (resulting from the breakdown of carnosine into its constituents, owing to the action of carnosinases present in the gastrointestinal tract and in plasma) into cells and the subsequent catalytic action of carnosine synthase to from carnosine, or *2)* the direct uptake of intact carnosine into cells. Once carnosine is inside the cells, it can be converted into its methylated or acetylated analogues. In our model, the first mechanism is virtually impossible to occur, because *CARNS1*$^{-/-}$ lack carnosine synthase; thus, the direct uptake of the intact dipeptide is the sole route for increased tissue carnosine in response to supplementation. Carnosine can be transported across cell membranes by proton-coupled oligopeptide transporters [50], namely PEPT1, PEPT2, PHT1, and PHT2. While PEPT1 and PEPT2 do not seem to be expressed in rodent muscle, PHT1 and PHT2 have been reported to be well expressed [39]. Our data also confirmed that both *PHT1* and *PHT2* genes are expressed in cardiac muscle, but their expression is relatively low in comparison with other constitutive genes (*YWHAZ* and *HMBS*). Nonetheless, muscle carnosine remained virtually absent in the *CARNS1*$^{-/-}$ rats after supplementation. The lack of meaningful increases in carnosine might be due to the low expression levels of these genes, or due to the fact that these transporters are unspecific and transport a wide variety of di- and tri-peptides and histidine [51]. In fact, very little is known as to whether carnosine can be transported in or out of the striated muscles, and our data indicates that carnosine synthesis via carnosine synthase is the major and most important mechanism for maintaining intracellular carnosine within normal levels. Owing to the inability of the transporters PHT1 and PHT2 to promote tissue carnosine accrual without the presence of a functional carnosine synthase, we were unable to further conduct rescue-of-function experiments, which we acknowledge is a limitation of our model.

To conclude, we developed and thoroughly described a novel *CARNS1*$^{-/-}$ rat strain; the results show that a primary function of HCDs in the cardiac muscle is the regulation of Ca^{2+} handling and EC coupling. The same function, however, seems not to apply in the skeletal muscle. HCDs seem to fulfill very specialised functions that are tissue specific. Our data, if replicated in humans, indicate that carnosine, anserine and their acetylated analogues could be promising therapeutic targets in cardiac diseases, especially because simple dietary interventions, can produce significant and consistent increases in their tissue content. While emerging evidence suggests that carnosine supplementation in patients with chronic heart failure can improve selected health outcomes [52], studies are still scarce, with high risk of bias [53] and lack proper mechanistic foundations. Advancing knowledge on the control of HCDs homeostasis in cardiac muscle is fundamental to develop effective nutritional therapies.

Funding sources

The study was funded by FAPESP (grant number 2014/11948-8 and 2019/25032-9). L.S.G was funded by CAPES. J.C.C, L.S.R, L.R.G.B were funded by FAPESP (grant numbers 2017/16540-5, 2020/04006-7 and

2017/11142-1). M.H.G, V.H.C and B.S.V were funded by FAPESP (CEPID REDOXOMA 2013/07937-8 and 2019/24899-9) and CNPq (grant number 301404/2016-0). L.C.M was a research fellow from CNPq and funded by FAPESP - research grant 2018/14544-6. B.G was funded by FAPESP (grant number 2013/14746-4 and 2017/13552-2).

Author contributions

G.G.A, L.S.G and J.C. designed research; L.S.G, L.P.S, T.R.S, J.C.C, A.L.F, J.N, L.J, A.A, L.S.R, L.R.G.B, M.E, I.C, D.S, A.C, V.H.C, B.S.V conducted experiments; L.C.M, B.G, W.T, M.H.G.M, I.L.B, M.C.I, J.C.B.F contributed new reagents or analytic tools; L.S.G, L.J, A.A, V.H.C, B.S.V, M.H.G.M, C.S, I.L.B, M.C.I, J.C.B.F, G.G. performed data analysis; G.G.A supervised the project; L.S.G, C.S and G.G.A wrote the paper; L.S.G, L.P.S, T.R.S, J.C.C, A.L.F, J.N, L.J, A.A, L.S.R, L.R.G.B, M.E, I.C, D.S, A.C, V.H.C; L.S.G, L.P.S, T.R.S, J.C.C, A.L.F, J.N, L.J, A.A, L.S.R, L.R.G.B, M.E, I.C, D.S, A.C, L.C.M, B.G, W.T, V.H.C, M.H.G.M, C.S, I.L.B, M.C.I, J.C.B.F, G.G.A revised the paper.

Declaration of competing interest

Although not directly related to this study, CS received funding to support a PhD studentship relating to the effects of carnosine on cardiac function from Natural Alternatives International; a company formulating and manufacturing customised nutritional supplements, including (Carnosyn SR™) beta-alanine. The same company has also provided CS with supplements for other studies free of charge and has contributed to the payment of open access publication charges for some manuscripts on beta-alanine supplementation. There are no other conflicts of interest to declare.

Acknowledgments

We thank Flamma S.p.A for providing carnosine supplement and Igor Longobardi for the help with Fig. 1 preparation (created with BioRender.com).

Appendix A. Supplementary data

Supplementary data to this article can be found online at https://doi.org/10.1016/j.redox.2021.102016.

References

[1] A.A. Boldyrev, G. Aldini, W. Derave, Physiology and pathophysiology of carnosine, Physiol. Rev. 93 (4) (2013) 1803–1845.
[2] J.J. O'Dowd, D.J. Robins, D.J. Miller, Detection, characterisation, and quantification of carnosine and other histidyl derivatives in cardiac and skeletal muscle, Biochim. Biophys. Acta 967 (2) (1988) 241–249.
[3] J. Drozak, M. Veiga-da-Cunha, D. Vertommen, V. Stroobant, E. Van Schaftingen, Molecular identification of carnosine synthase as ATP-grasp domain-containing protein 1 (ATPGD1), J. Biol. Chem. 285 (13) (2010) 9346–9356.
[4] A. Boldyrev, H. Abe, Metabolic transformation of neuropeptide carnosine modifies its biological activity, Cell. Mol. Neurobiol. 19 (1) (1999) 163–175.
[5] L. Blancquaert, S.P. Baba, S. Kwiatkowski, J. Stautemas, S. Stegen, S. Barbaresi, W. Chung, A.A. Boakye, J.D. Hoetker, A. Bhatnagar, J. Delanghe, B. Vanheel, M. Veiga-da-Cunha, W. Derave, I. Everaert, Carnosine and anserine homeostasis in skeletal muscle and heart is controlled by beta-alanine transamination, J. Physiol. 594 (17) (2016) 4849–4863.
[6] R.C. Harris, M.J. Tallon, M. Dunnett, L. Boobis, J. Coakley, H.J. Kim, J. L. Fallowfield, C.A. Hill, C. Sale, J.A. Wise, The absorption of orally supplied beta-alanine and its effect on muscle carnosine synthesis in human vastus lateralis, Amino Acids 30 (3) (2006) 279–289.
[7] M. Tanokura, M. Tasumi, T. Miyazawa, 1H nuclear magnetic resonance studies of histidine-containing di- and tripeptides. Estimation of the effects of charged groups on the pKa value of the imidazole ring, Biopolymers 15 (2) (1976) 393–401.
[8] H. Abe, Role of histidine-related compounds as intracellular proton buffering constituents in vertebrate muscle, Biochemistry, Biokhimiia 65 (7) (2000) 757–765.
[9] B. Saunders, K. Elliott-Sale, G.G. Artioli, P.A. Swinton, E. Dolan, H. Roschel, C. Sale, B. Gualano, beta-alanine supplementation to improve exercise capacity and performance: a systematic review and meta-analysis, Br. J. Sports Med. 51 (8) (2017) 658–669.
[10] E. Dolan, B. Saunders, W.S. Dantas, I.H. Murai, H. Roschel, G.G. Artioli, R. Harris, J. Bicudo, C. Sale, B. Gualano, A comparative study of hummingbirds and chickens provides mechanistic insight on the histidine containing dipeptide role in skeletal muscle metabolism, Sci. Rep. 8 (1) (2018) 14788.
[11] R. Ghodsi, S. Kheirouri, Carnosine and advanced glycation end products: a systematic review, Amino Acids 50 (9) (2018) 1177–1186.
[12] V.H. Carvalho, A.H.S. Oliveira, L.F. de Oliveira, R.P. da Silva, P. Di Mascio, B. Gualano, G.G. Artioli, M.H.G. Medeiros, Exercise and beta-alanine supplementation on carnosine-acrolein adduct in skeletal muscle, Redox Biol. 18 (2018) 222–228.
[13] M.A. Batrukova, A.M. Rubtsov, Histidine-containing dipeptides as endogenous regulators of the activity of sarcoplasmic reticulum Ca-release channels, Biochim. Biophys. Acta 1324 (1) (1997) 142–150.
[14] C. Lamont, D.J. Miller, Calcium sensitizing action of carnosine and other endogenous imidazoles in chemically skinned striated muscle, J. Physiol. 454 (1992) 421–434.
[15] J.J. O'Dowd, M.T. Cairns, M. Trainor, D.J. Robins, D.J. Miller, Analysis of carnosine, homocarnosine, and other histidyl derivatives in rat brain, J. Neurochem. 55 (2) (1990) 446–452.
[16] G.A. McFarland, R. Holliday, Retardation of the senescence of cultured human diploid fibroblasts by carnosine, Exp. Cell Res. 212 (2) (1994) 167–175.
[17] F. Gaunitz, A.R. Hipkiss, Carnosine and cancer: a perspective, Amino Acids 43 (1) (2012) 135–142.
[18] L. Mora, M.A. Sentandreu, F. Toldra, Hydrophilic chromatographic determination of carnosine, anserine, balenine, creatine, and creatinine, J. Agric. Food Chem. 55 (12) (2007) 4664–4669.
[19] T. Nemkov, A. D'Alessandro, K.C. Hansen, Three-minute method for amino acid analysis by UHPLC and high-resolution quadrupole orbitrap mass spectrometry, Amino Acids 47 (11) (2015) 2345–2357.
[20] J.C. Ferreira, N.P. Rolim, J.B. Bartholomeu, C.A. Gobatto, E. Kokubun, P.C. Brum, Maximal lactate steady state in running mice: effect of exercise training, Clin. Exp. Pharmacol. Physiol. 34 (8) (2007) 760–765.
[21] B. Kalmar, L. Greensmith, Activation of the heat shock response in a primary cellular model of motoneuron neurodegeneration-evidence for neuroprotective and neurotoxic effects, Cell. Mol. Biol. Lett. 14 (2) (2009) 319–335.
[22] B.R. MacIntosh, S.P. Esau, R.J. Holash, J.R. Fletcher, Procedures for rat in situ skeletal muscle contractile properties, JoVE : JoVE 56 (2011) e3167.
[23] V. De Salles Painelli, K.M. Nemezio, A.J. Pinto, M. Franchi, I. Andrade, L.A. Riani, B. Saunders, C. Sale, R.C. Harris, B. Gualano, G.G. Artioli, High-intensity interval training augments muscle carnosine in the absence of dietary beta-alanine intake, Med. Sci. Sports Exerc. 50 (11) (2018) 2242–2252.
[24] S. Gao, D. Ho, D.E. Vatner, S.F. Vatner, Echocardiography in mice, Curr. Protoc. Mouse Biol. 1 (2011) 71–83.
[25] L.H.M. Bozi, A.P.C. Takano, J.C. Campos, N. Rolim, P.M.M. Dourado, V. A. Voltarelli, U. Wisloff, J.C.B. Ferreira, M.L.M. Barreto-Chaves, P.C. Brum, Endoplasmic reticulum stress impairs cardiomyocyte contractility through JNK-dependent upregulation of BNIP3, Int. J. Cardiol. 272 (2018) 194–201.
[26] D.V. Cancherini, B.B. Queliconi, A.J. Kowaltowski, Pharmacological and physiological stimuli do not promote Ca(2+)-sensitive K+ channel activity in isolated heart mitochondria, Cardiovasc. Res. 73 (4) (2007) 720–728.
[27] J.C.B. Ferreira, J.C. Campos, N. Qvit, X. Qi, L.H.M. Bozi, L.R.G. Bechara, V. M. Lima, B.B. Queliconi, M.H. Disatnik, P.M.M. Dourado, A.J. Kowaltowski, D. Mochly-Rosen, A selective inhibitor of mitofusin 1-betaIIPKC association improves heart failure outcome in rats, Nat. Commun. 10 (1) (2019) 329.
[28] J.A. Durlak, How to select, calculate, and interpret effect sizes, J. Pediatr. Psychol. 34 (9) (2009) 917–928.
[29] M.J. Cripps, K. Hanna, C. Lavilla Jr., S.R. Sayers, P.W. Caton, C. Sims, L. De Girolamo, C. Sale, M.D. Turner, Carnosine scavenging of glucolipotoxic free radicals enhances insulin secretion and glucose uptake, Sci. Rep. 7 (1) (2017) 13313.
[30] B. Saunders, V. De Salles Painelli, L.F. De Oliveira, V. Da Eira Silva, R.P. Da Silva, L. Riani, M. Franchi, L.S. Goncalves, R.C. Harris, H. Roschel, G.G. Artioli, C. Sale, B. Gualano, Twenty-four weeks of beta-alanine supplementation on carnosine content, related genes, and exercise, Med. Sci. Sports Exerc. 49 (5) (2017) 896–906.
[31] T.L. Dutka, G.D. Lamb, Effect of carnosine on excitation-contraction coupling in mechanically-skinned rat skeletal muscle, J. Muscle Res. Cell Motil. 25 (3) (2004) 203–213.
[32] R. Hannah, R.L. Stannard, C. Minshull, G.G. Artioli, R.C. Harris, C. Sale, beta-Alanine supplementation enhances human skeletal muscle relaxation speed but not force production capacity, J. Appl. Physiol. 118 (5) (2015) 604–612.
[33] E.P. Debold, Recent insights into the molecular basis of muscular fatigue, Med. Sci. Sports Exerc. 44 (8) (2012) 1440–1452.
[34] C.H. Cho, J.S. Woo, C.F. Perez, E.H. Lee, A focus on extracellular Ca(2+) entry into skeletal muscle, Exp. Mol. Med. 49 (9) (2017) e378.
[35] P. Kosger, G. Ozdemir, A. Yildirim, B. Ucar, Z. Kilic, Early myocardial changes in normotensive children of hypertensive parents: a tissue Doppler study, Hypertens. Res. : Off. J. Jpn. Soc. Hypertens. 41 (11) (2018) 897–903.
[36] C. Tei, K.S. Dujardin, D.O. Hodge, R.A. Kyle, A.J. Tajik, J.B. Seward, Doppler index combining systolic and diastolic myocardial performance: clinical value in cardiac amyloidosis, J. Am. Coll. Cardiol. 28 (3) (1996) 658–664.
[37] J.N. Peoples, A. Saraf, N. Ghazal, T.T. Pham, J.Q. Kwong, Mitochondrial dysfunction and oxidative stress in heart disease, Exp. Mol. Med. 51 (12) (2019) 1–13.

[38] V.D. Prokopieva, E.G. Yarygina, N.A. Bokhan, S.A. Ivanova, Use of carnosine for oxidative stress reduction in different pathologies, Oxidative Med. Cell. Longev. 2016 (2016) 2939087.
[39] I. Everaert, S. Stegen, B. Vanheel, Y. Taes, W. Derave, Effect of beta-alanine and carnosine supplementation on muscle contractility in mice, Med. Sci. Sports Exerc. 45 (1) (2013) 43–51.
[40] C.W. Botka, T.W. Wittig, R.C. Graul, C.U. Nielsen, K. Higaka, G.L. Amidon, W. Sadee, Human proton/oligopeptide transporter (POT) genes: identification of putative human genes using bioinformatics, AAPS PharmSci 2 (2) (2000) E16.
[41] J. Zhao, D.J. Conklin, Y. Guo, X. Zhang, D. Obal, L. Guo, G. Jagatheesan, K. Katragadda, L. He, X. Yin, M.A.I. Prodhan, J. Shah, D. Hoetker, A. Kumar, V. Kumar, M.F. Wempe, A. Bhatnagar, S.P. Baba, Cardiospecific overexpression of ATPGD1 (carnosine synthase) increases histidine dipeptide levels and prevents myocardial ischemia reperfusion injury, J. Am. Heart Assoc. 9 (12) (2020), e015222.
[42] D.M. Bers, Cardiac excitation-contraction coupling, Nature 415 (6868) (2002) 198–205.
[43] A. Dayal, K. Schrotter, Y. Pan, K. Fohr, W. Melzer, M. Grabner, The Ca(2+) influx through the mammalian skeletal muscle dihydropyridine receptor is irrelevant for muscle performance, Nat. Commun. 8 (1) (2017) 475.
[44] M. Nabauer, G. Callewaert, L. Cleemann, M. Morad, Regulation of calcium release is gated by calcium current, not gating charge, in cardiac myocytes, Science 244 (4906) (1989) 800–803.
[45] G.P. Zaloga, P.R. Roberts, T.E. Nelson, Carnosine, A novel peptide regulator of intracellular calcium and contractility in cardiac muscle, New horizons 4 (1) (1996) 26–35.
[46] R.L. Moss, G.G. Giulian, M.L. Greaser, The effects of partial extraction of TnC upon the tension-pCa relationship in rabbit skinned skeletal muscle fibers, J. Gen. Physiol. 86 (4) (1985) 585–600.
[47] P. Swietach, J.B. Youm, N. Saegusa, C.H. Leem, K.W. Spitzer, R.D. Vaughan-Jones, Coupled Ca2+/H+ transport by cytoplasmic buffers regulates local Ca2+ and H+ ion signaling, Proc. Natl. Acad. Sci. U.S.A. 110 (22) (2013) E2064–E2073.
[48] A.A. Boldyrev, A.M. Dupin, E.V. Pindel, S.E. Severin, Antioxidative properties of histidine-containing dipeptides from skeletal muscles of vertebrates, Comp. Biochem. Physiol B Comp. Biochem. 89 (2) (1988) 245–250.
[49] A.A. Boldyrev, A.M. Dupin, M.A. Batrukova, N.I. Bavykina, G.A. Korshunova, P. Shvachkin Yu, A comparative study of synthetic carnosine analogs as antioxidants, Comp. Biochem. Physiol B Comp. Biochem. 94 (2) (1989) 237–240.
[50] H. Oppermann, M. Heinrich, C. Birkemeyer, J. Meixensberger, F. Gaunitz, The proton-coupled oligopeptide transporters PEPT2, PHT1 and PHT2 mediate the uptake of carnosine in glioblastoma cells, Amino Acids 51 (7) (2019) 999–1008.
[51] D.J. Lindley, S.M. Carl, S.A. Mowery, G.T. Knipp, The evaluation of peptide/histidine transporter 1 (Pht1) function: uptake kinetics utilizing a cos-7 stably transfected cell line, Rev. Mex. Ciencias Farm. 42 (4) (2011) 57–65.
[52] C. Lombardi, V. Carubelli, V. Lazzarini, E. Vizzardi, T. Bordonali, C. Ciccarese, A. I. Castrini, A. Dei Cas, S. Nodari, M. Metra, Effects of oral administration of orodispersible levo-carnosine on quality of life and exercise performance in patients with chronic heart failure, Nutrition 31 (1) (2015) 72–78.
[53] I. Hopper, C. Connell, T. Briffa, C.G. De Pasquale, A. Driscoll, P.M. Kistler, P. S. Macdonald, A. Sindone, L. Thomas, J.J. Atherton, Nutraceuticals in patients with heart failure: a systematic review, J. Card. Fail. 26 (2) (2020) 166–179.